9. Determination of Forward Electron Transfer Rates of Site-Directed Mutants in a Putative Electron Transfer Pathway from A_0 through A_1 to F_X

As discussed in the previous Chapter 8, the issue of electron transfer directionality can be addressed by the use of point mutants and the combination of time resolved EPR and optical spectroscopy. The initial electron transfer steps are difficult to observe directly because the trapping of the excitation energy in the antenna Chls masks these early events in optical spectroscopy [20]. In contrast, the subsequent electron transfer from phylloquinone A_1 to the iron-sulphur center F_X can be detected by both optical and TR-EPR spectroscopy and provides a convenient way to study the kinetics and pathway of electron transfer.

In this chapter EPR and optical kinetic studies of mutants in and around the quinone binding sites of PS I are reported. The premise of these experiments is that a change in the environment of the quinone should lead to a change in its redox potential, which, in turn, should translate to a change in the forward electron transfer kinetics from the quinone to the iron-sulphur clusters.

In the preceding Chapter 8, it was demonstrated that the point mutations $W697F_{PsaA}$, $W677F_{PsaB}$, $S692C_{PsaA}$, $S672C_{PsaB}$, $R694A_{PsaA}$ and $R674A_{PsaB}$ cause only subtle structural and electronic changes, at the same time they are expected to influence the electron transfer rate. Only the electron transfer in the branch containing the mutation will be affected. The $R694A_{PsaA}$ and $R674A_{PsaB}$ mutants on the other hand may affect both branches because each is involved in a salt bridge from the **jk**-surface loop to $G572_{PsaB}$ ($G585_{PsaA}$) in the respective F_X binding loop [93]. In other words, this residue acts at the level of F_X where it ties together the region of the quinone with that of the iron-sulphur cluster. Mutations of these arginines cause a change in the properties of F_X. The results presented in this chapter address the issue of directionality and biphasic kinetics and

support the conclusion that in *Synechocystis* sp. PCC 6803, the majority of electrons proceed along PsaA-side of cofactors in PS I.

9.1 Time-Resolved Optical Measurements in Whole Cells and Isolated PS I Complexes

Our main effort focuses on applying a set of complementary spectroscopic techniques to characterize transient charge separated states in a comparative study of the influence of mutations near the A_1 binding site. Data of optical absorbance difference spectroscopy in the near UV/blue in both whole cells and isolated PS I complexes are compared with those of transient EPR spectroscopy [95]. Optical studies were performed by Mariana Guergova-Kuras at Institut de Biologie Physico-Chimique, Paris, France and Klaus Brettel at Service de Bioénergétique, Cedex, France.

Measurements of flash-induced difference spectrum A_1^-/A_1 have been done in the whole mutant cells and in the PS I particles (trimers) prepared from cells. This has the purpose to control possible preparation induced effects. The advantage of studying kinetic processes in whole cells is that there is no potential damage to the acceptor cofactors as a result of detergent solubilization of the thylakoid membranes. The disadvantage is that the cells are actively growing and dividing, and PS I complexes may be present in a number of developing stages, including those undergoing assembly and degradation. To minimize any potential for heterogenity due to turnover and to reduce effects of background absorption and competing photoprocesses in larger antenna systems, studies were performed on whole cells and purified PS I complexes. Ideally, the kinetic results should match in both studies.

The flash-induced difference spectrum of A_1^-/A_1 shows a broad absorption increase between 340 nm and 400 nm [28, 96]. Measurements in PS I complexes were made at the maximum of 380 nm (in addition data were taken at 480 nm). An absorption band in the visible region that is assigned to A_1^-/A_1 absorption changes but is likely to be contaminated by other processes.

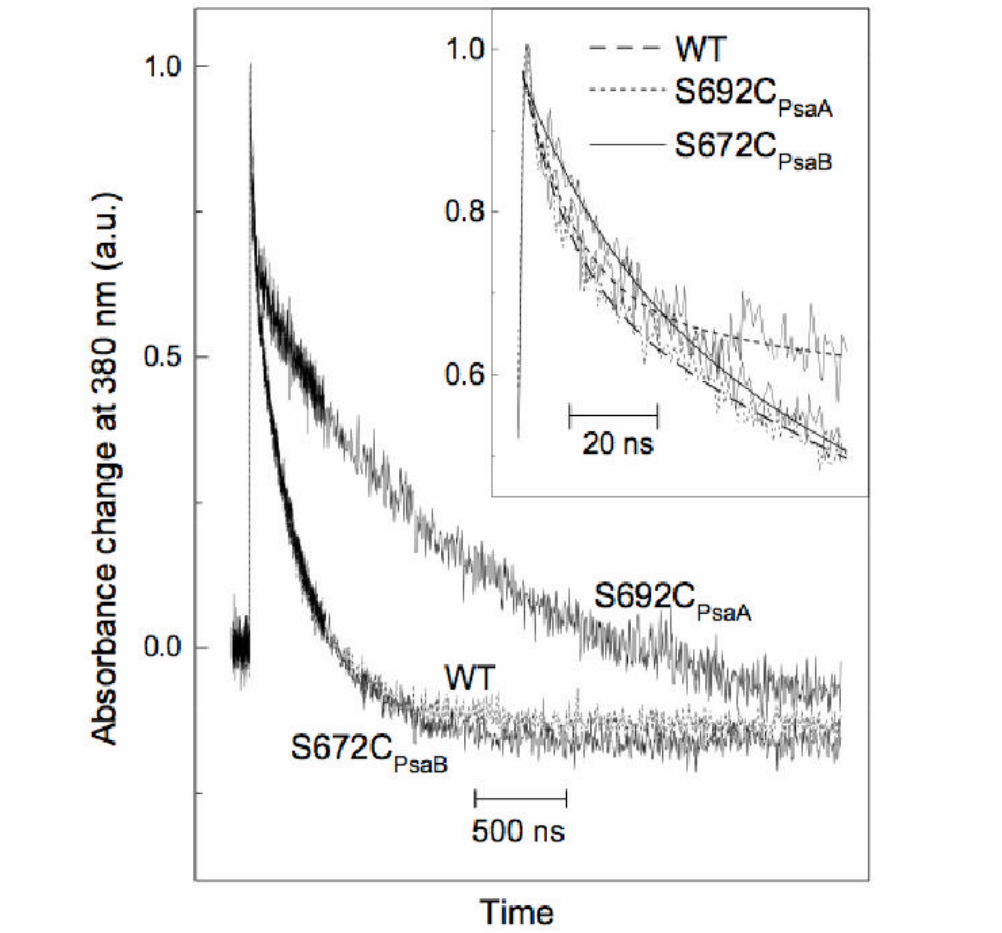

Figure 9.1 Kinetics of flash-induced absorbance changes at 380 nm in isolated PS I complexes from wild-type (WT), $S692C_{PsaA}$ and $S672C_{PsaB}$ at room temperature. The inset shows the same traces on an expanded scale, together with the best bi-exponential fits (dashed line, wild-type; dotted line, $S692C_{psaA}$; solid line, $S672C_{PsaB}$). The signals were arbitrarily normalized to simplify the comparison. The maximal amplitudes correspond to absorbance changes of 6.7×10^{-4} for the wild-type (optical density of the sample at 679 nm, $OD_{679} = 0.76$), 8.9×10^{-4} for $S692C_{PsaA}$ ($OD_{679} = 1.02$), and 8.7×10^{-4} for $S672C_{PsaB}$ ($OD_{679} = 0.98$). For experimental details see [95].

For technical reasons, measurements in whole cells were performed at the less optimal wavelengths of 390 nm and 400 nm. In all cases two kinetic phases were found: fast phase in the time range of 10-30 ns and slow phase in the time range of hundred nanoseconds.

For example, Figure 9.1 depicts the decay of flash-induced absorbance changes at 380 nm in isolated PS I complexes from wild-type (WT), $S692C_{PsaA}$ and $S672C_{PsaB}$ at room temperature. The inset shows the same traces on an expanded scale, together with the best bi-exponential fits. The present of fast phase can be clearly seen. In Figure 9.1 it is clearly visible that the electron transfer kinetic slows down when the mutation is in the PsaA branch ($S692C_{PsaA}$). In the PsaA-side mutant $S692C_{PsaA}$ the lifetime of the slow kinetic phase is increased by a factor of about 4. The insert shows that the fast phase is resolved only at early time and slows down when the mutation is located in the corresponding (symmetric) PsaB branch ($S672C_{PsaB}$). Surprisingly, within experimental error the lifetime of the fast kinetic phase in the whole cells does not appear to be lengthened at either detection wavelength.

For the mutants $W697F_{PsaA}$ and $W677F_{PsaB}$, the kinetics in isolated PS I complexes are similar to those obtained in whole cells and Ser to Cys mutants followed the same trends, *i.e.*, only the slower phase was slowed consistently in the PsaA-side mutant, while only the faster phase was slowed in the PsaB-side mutant, however to a quite different degree. Within experimental accuracy the relative amplitudes of the two phases appeared to be independent of these mutations. Similar results were observed in mutants of *Chlamydomonas reinhardtii* [90], in which the mutation of Trp to Phe on PsaA increased the lifetime of the slow phase while the corresponding (symmetric) mutation on PsaB slowed down the fast phase. For more detailed information about the fast and slow kinetic phases determined for the whole cells and PS I particles and their changes upon the mutations see Tables I and II in [95].

Together the data show that for all mutations expected to influence on the electron transfer in the PsaA branch, the slow kinetic phase is slowed significantly. It is less clear whether such a trend holds for the fast kinetic phase. The measured lifetimes for the Trp mutants suggest that only the fast phase is affected by mutations on the PsaB branch.

However, for Ser mutants, mutations in the PsaB branch showed a significant slowing of the fast phase only in isolated PS I and not in whole cells, although the corresponding mutations in the PsaA branch consistently affect the slow phase in both types of samples.

9.2 Room temperature electron spin polarized EPR spectra at X-Band

Room temperature Transient EPR experiments were performed parallel by Alfia Valieva and Art van der Est at Brock University, St. Catherines, Canada and in our laboratory. Kinetically separated electron spin polarized EPR spectra at room temperature are compared in Figure 9.2 for the wild-type and the mutants. The kinetically separated spectra were obtained from the complete time/field data sets by fitting the kinetic equation (see Chapter 5, section 5.6) to all individual transients as described in [27]; positive signals correspond to absorption (A) and negative signals correspond to emission (E). As the electron is transferred to the iron-sulphur clusters, the initial E/A/E polarization pattern due to $P_{700}^{+}A_1^{-}$ changes to the primarily emissive P_{700}^{+} contribution of the $P_{700}^{+}FeS^{-}$ spectrum. In Figure 9.2 the overall shape of all spectra of the $W697F_{PsaA}$, $W677F_{PsaB}$, $S692C_{PsaA}$, $S672C_{PsaB}$, $R694A_{PsaA}$ and $R674A_{PsaB}$ mutants are quite similar, in particular for the B-site mutants they are nearly identical to wild type. Otherwise, some small but significant changes are observed as a result of the mutations. The spectral differences are most obvious in the case of the $W697F_{PsaA}$ mutant (left column top), which shows a more pronounced hyperfine structure in comparison to the wild type. This is the same result as observed in the low temperature transient EPR spectra (Figure 8.2) and in the pulsed ENDOR (Figure 8.5). The spectra of the $S692C_{PsaA}$ mutant (middle left) and the $R694A_{PsaA}$ mutant (bottom left) also show some indication of the weaker hyperfine structure seen at low temperature; however, the lower signal to noise ratio at room temperature does not allow the effect to be detected clearly. The temperature dependence of the spectra was also measured and no significant differences in the polarization patterns were observed between 80 K and room temperature.

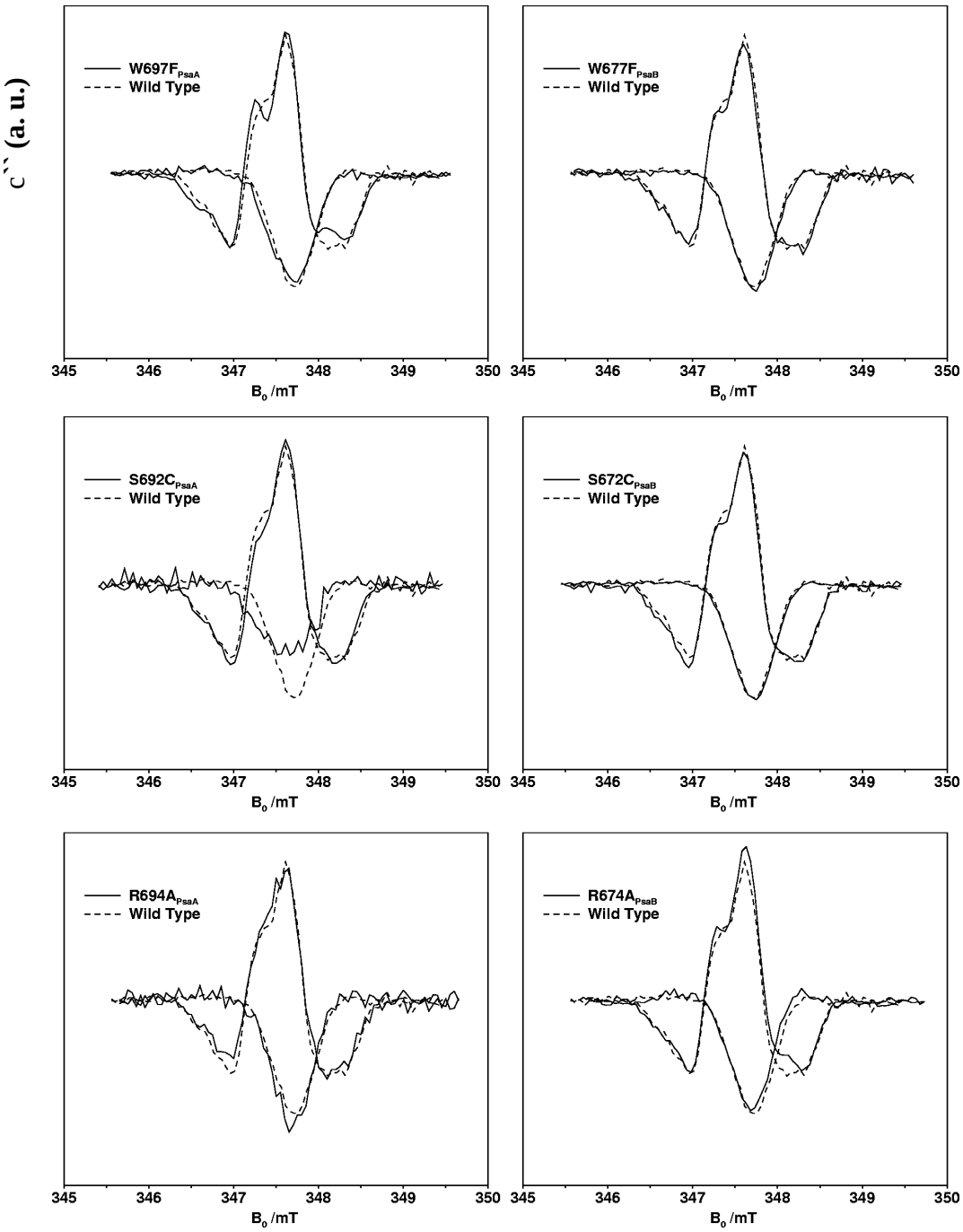

Figure 9.2. Kinetically separated transient EPR spectra of PS I at room temperature (X-band) with point mutations in PsaA (left) and PsaB (right). The spectra are due to $P_{700}^{+}A_1^{-}$ (E/A/E pattern) and $P_{700}^{+}FeS^{-}$ (emissive spectrum) and have been extracted from the time/field datasets by fitting the individual transients. The solid curves are from the mutants and the dashed curves are the corresponding spectra from wild type PS I. Top left $W667F_{PsaA}$, top right $W677F_{PsaB}$, middle left $S692C_{PsaA}$, middle right $S672C_{PsaB}$, bottom left $R694A_{PsaA}$, bottom right $R674A_{PsaB}$.

The correspondence between the low temperature and room temperature spectra of the Trp mutants (and the other mutants within the limitation of the signal to noise) is important because it shows that conclusions based on the low temperature spectra are relevant for PS I under physiological conditions as well.

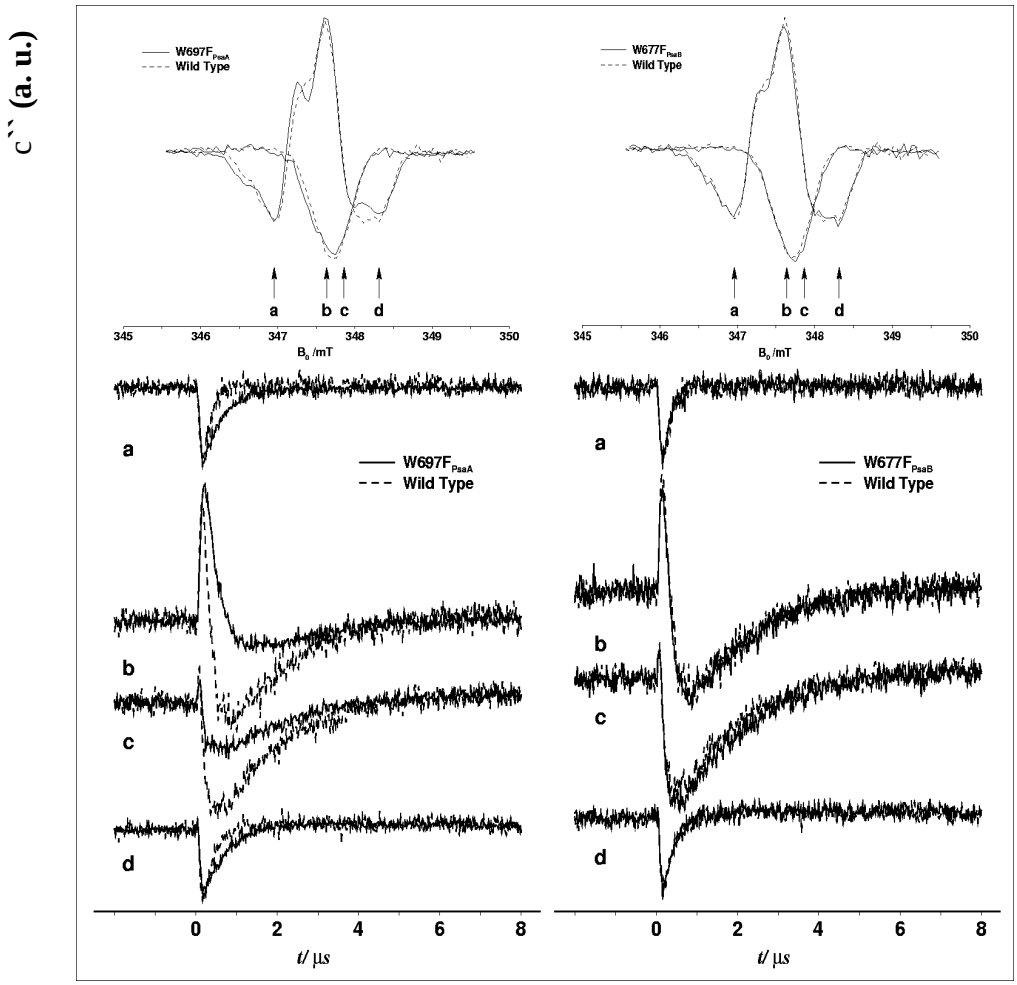

Figure 9.3 Transient EPR kinetic traces of PS I (full line) at room temperature and X-band from the $W697F_{PsaA}$ mutant (left) and the $W677F_{PsaB}$ mutant (right) compared to wild type (broken line). The field positions at which the transients were taken are indicated by arrows labeled a-d below the kinetically separated spectra of the $P_{700}^{+}A_1^{-}$ and $P_{700}^{+}FeS^{-}$ states shown at the top of the figure. The spectra were obtained using the fitting procedure described in [27].

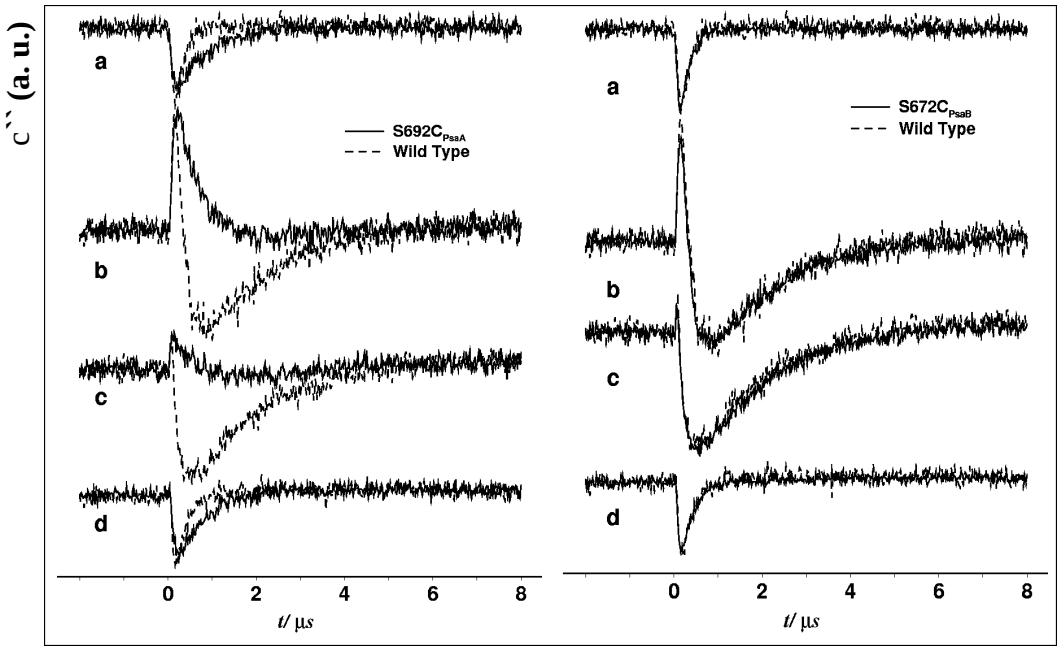

Figure 9.4 Transient EPR kinetics of the S692C$_{PsaA}$ mutant (left) and S672C$_{PsaB}$ mutants (right) compared to wild type PS I. Experimental conditions and the field positions are the same as shown in Figure 9.3. The solid curves are from the mutants and the dashed curves are from wild type.

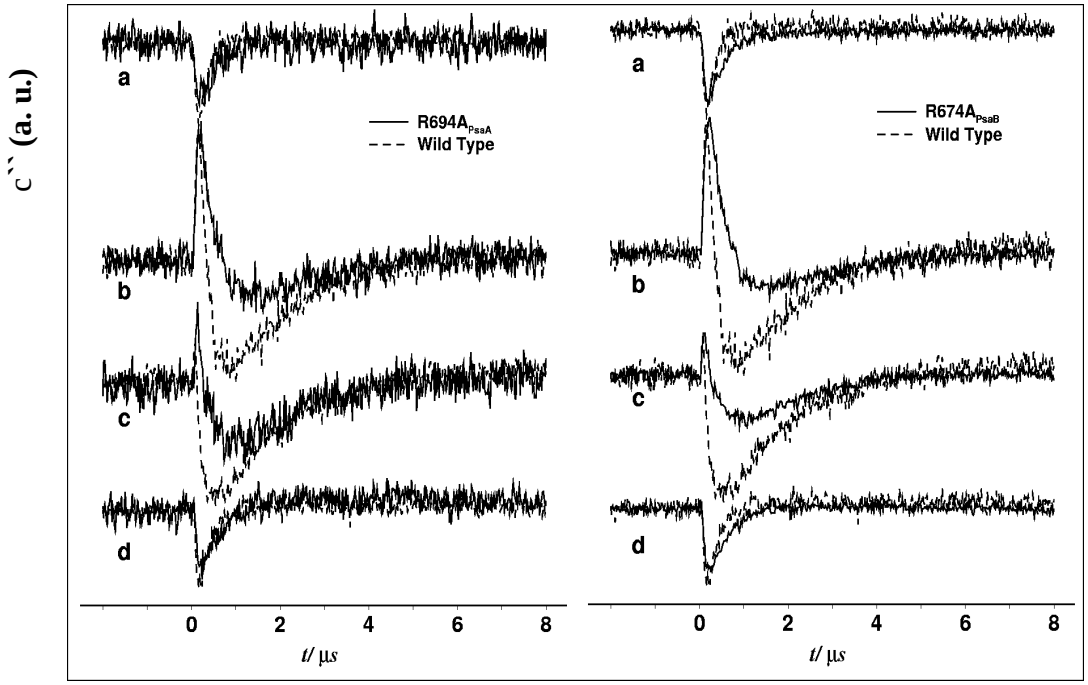

Figure 9.5 Transient EPR kinetics of the R694AC$_{PsaA}$ mutant (left) and R674A$_{PsaB}$ mutants (right) compared to wild type PS I. Experimental conditions and the field positions are the same as shown in Figure 9.3. The solid curves are from the mutants and the dashed curves are from wild type.

The data shown in Figure 9.2 are from isolated PS I complexes. It is known that for some species [29], the isolation procedure can have an influence on the observed biphasic kinetics, in particular, it increases the fast phase. To ensure that such effects are not occurring in these samples, we performed transient EPR experiments also on whole cells of wild type *Synechocystis* sp. PCC 6803 and the spectra (not shown) are indistinguishable from the spectra of isolated wild-type PS I complexes.

Figure 9.3 compares EPR-transients of PS I trimers of the wild type and of the $W697F_{PsaA}$ (left) and $W677F_{PsaB}$ (right) mutants, respectively. The transients are taken at selected field positions as indicated by arrows in the spectra at the top of the figure. In the low field region, position **a**, only A_1^- contributes to the $P_{700}^+A_1^-$ spectrum, so that the decay of the EPR signal at this field position reflects the forward electron transfer from A_1^- to F_X, provided that it is significantly faster than the decay of the spin polarization (Table 9.1). At the other field positions, the contributions from both P_{700}^+ and A_1^- to the consecutive RP spectra are overlapped. As is evident from the kinetic traces, the transients from the $W697F_{PsaA}$ mutant (Figure 9.3, left) are significantly different from the wild type and the forward electron transfer is slowed down for this mutant. A fit of the data yields a lifetime for the electron transfer of $\tau = 640 \pm 50$ ns in the $W697F_{PsaA}$ mutant compared to $\tau = 240 \pm 50$ ns in the wild type. In contrast, the transients and spectra from the $W677F_{PsaB}$ mutant (Figure 9.3, right) are indistinguishable from wild type PS I.

Figure 9.4 shows corresponding transients for the $S692C_{PsaA}$ and $S672C_{PsaB}$ mutants. They show similar kinetic behavior to the Trp mutants (Figure 9.3) but the kinetic slow-down effect of the PsaA mutation is even more pronounced. A fit of the dataset yields a lifetime of $\tau = 1290 \pm 50$ ns for the $S692C_{PsaA}$ mutant. In this case the lifetime of the electron transfer from A_1^- to F_X and the lifetime of the spin polarization happen to be approximately equal, see Table 9.1, which causes difficulties in extracting kinetically

separated spectra. Note that the weaker $P_{700}^{+}FeS^{-}$ spectrum for the $S692C_{PsaA}$ mutant (middle left) in Figure 9.2 is an artefact.

Thus, consistent with the optical data, a slowing of the slow phase is observed as a result of the mutations in the PsaA-branch quinone binding site. The corresponding PsaB branch mutations do not cause any detectable change in the spin polarization.

Room temperature transients of the $R694A_{PsaA}$ and $R674_{PsaB}$ mutants are shown in Figure 9.5. Surprisingly the kinetic slow down is observed in the same way for both the A- and B-side mutants. The qualitative analysis of the datasets yields almost identical values for the forward electron transfer rate from A_1^{-}: $\tau = 640 \pm 50$ ns and $\tau = 680 \pm 50$ ns. The optical absorbance changes in whole cells of the $R674A_{PsaB}$ mutant also show an increase in the lifetime of the slow phase but the lifetime obtained is roughly a factor of two longer [95].

Table 9.1 Kinetic Analysis of TR EPR spectra at 260 K and room temperature

	Room temperature[a]		260 K
	τ_{ET}(ns)	τ_{spin}(ns)[b]	τ_{ET}(ns)
WT	240	1440	840±50
PsaA W697F	640	1360	1820±50
PsaB W677F	240	1670	840±50
PsaA S692C	1290	1350	3020±100
PsaB S672C	220	1500	840±50
PsaA R694A	640	1360	1000±50
PsaB R674A	680	1340	1100±50

[a]Estimated error in all values ±20%, [b]Effective relaxation times for microwave power 10 mW. At 260K spin relaxation rates are too slow to be reliably evaluated.

The origin of this difference in the observed lifetimes is unclear but it may be simply related to temperature differences between the two experiments. The fact that the slowing of the electron transfer rate obtained from the EPR experiments is the same for both the PsaA- and PsaB-branch mutants can be easily rationalized by making the reasonable assumption that the mutations primarily affect the redox potential of F_X. However, the optical data show no effect on the fast phase in the $R674A_{PsaB}$ mutant. In addition, the $R694A_{PsaA}$ mutation leads to changes in the spin density on A_1^- as observed in low temperature ENDOR and transient EPR experiments (see previous Chapter 8 and Figure 8.5). Hence it is likely that properties other than the redox potential of F_X are also influenced by mutation of these Arg residues.

The values of the optically determined lifetimes of the slow phase for the mutants [95] are in reasonable qualitative agreement with the values determined from the transient EPR experiments summarized in Table 9.1. However, the optical experiments for the whole cells give lifetimes that are consistently longer [95]. This is likely a result of a difference in ‘room temperature’ between the experiments. The spin relaxation can also influence the evaluation of lifetimes obtained from the EPR transients; however, spin polarisation decay corresponds mainly to the electron transfer and the relaxation rate is obtained from extrapolation to zero microwave power [63]. Since no significant dependence on the microwave power was found the signal decay is given by electron transfer rate and correct electron transfer lifetimes can be determined.

Both the optical and the transient EPR data show that the slow kinetic phase is associated with electron transfer along the PsaA branch. However, no clear influence from the fast kinetic phase observed optically is detectable in the room temperature EPR so far. As discussed in [32] if the two phases would correspond to two fractions in the sample

with different rates of electron transfer from A_1^- to F_X, then both fractions contribute to the spectra and at least the spin polarization for $P_{700}^+(FeS)^-$ should be observed. The reasonable assumption has to be made that the spin polarisation due to P_{700}^+ part in $P_{700}^+(FeS)^-$ lives equally long whether it is coming from either of the two branches. Thus it should contribute the radical pair signal at early time, if the fast electron transfer really takes place. To look into more details of the early time behaviour of the radical pair signal and to find the possible contribution from the fast phase generated P_{700}^+, the TR-EPR experiments were done at 260K.

9.3 EPR Studies of the Slowing of A_1^- Oxidation at 260 K

At temperatures between 260 and 300 K, samples remain quasiliquid and charge separation between P_{700} and F_A/F_B remains reversible in wild-type PS I. The slow phase of forward electron transfer as measured by absorbance changes at 380 nm in PS I from *Synechococcus elongatus* [97] follows Arrhenius behaviour with an activation energy of 220±20 meV so that it is slowed by a factor of about 3 at 260 K compared to room temperature. For the other species *Synechocystis sp*., however, an activation energy 110 meV was determined [98]. If the fast and slow kinetic phases differ only as a result of different activation energies, the fast component could have lower activation energy and therefore weaker temperature dependence.

Transient EPR data were taken below room temperature but above ~200 K to study the influence of the mutations on the activation energy and to possibly separate contributions to the spin polarization from the fast phase, depending on how it changes with temperature. The only difference in the experimental conditions between the optical and EPR measurements was the presence of high glycerol concentration in samples subjected to optical study. As soon as temperature in our TR-EPR kinetic experiments

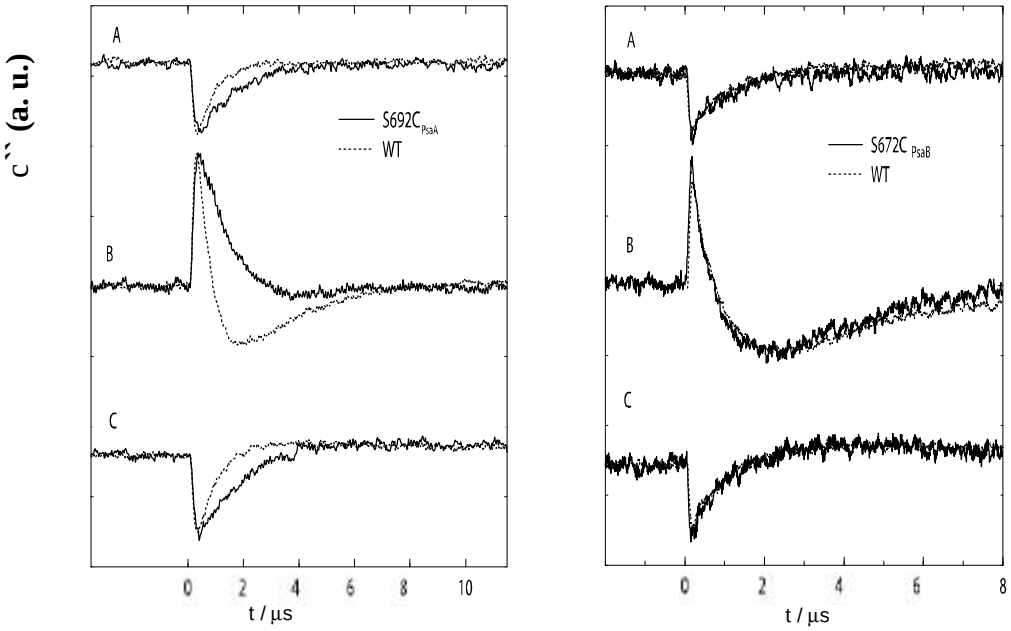

Figure 9.6 Transient EPR kinetic traces at selected magnetic field positions of the $S692C_{PsaA}$ mutant (left) and $S672C_{PsaB}$ mutant (right) compared to wild type PS I at 260K. The field positions are the same as shown in Figure 9.4 except that curve C corresponds to curve d. The solid curves are from the mutants and the dashed curves are from wild type.

nether was lower than the glycerol glass transition point we can assume the same behaviour for samples in optical and EPR experiments.

The EPR kinetic transients taken at 260 K are shown in Figures 9.6 and the electron transfer lifetimes evaluated from the transient EPR datasets are given in Table 9.1. The kinetics of A_1 oxidation are slowed by roughly the same factor of around two to three compared with room temperature for all of the samples. Thus, none of the mutations appears to have a large impact on the activation energy associated with the slow phase of electron transfer. In any case, the kinetics of A_1^- oxidation in the $W677F_{PsaB}$ and $S672C_{PsaB}$ mutants remain identical to those of the wild-type at 260 K.

The possible influence of the fast kinetic phase on the spin polarization patterns is investigated in Figure 9.7 which shows early spectra in four successive 16 ns time windows for the wild type and the $S672C_{PsaB}$ and $S692C_{PsaA}$ mutants. In general, the polarization patterns of spin-correlated radical pairs exhibit lifetime- or Fourier-broadening as well as coherence effects due to transient nutations, quantum beats and envelope modulation [51, 99, 100, 101]. Coherence effects do not make significant contributions

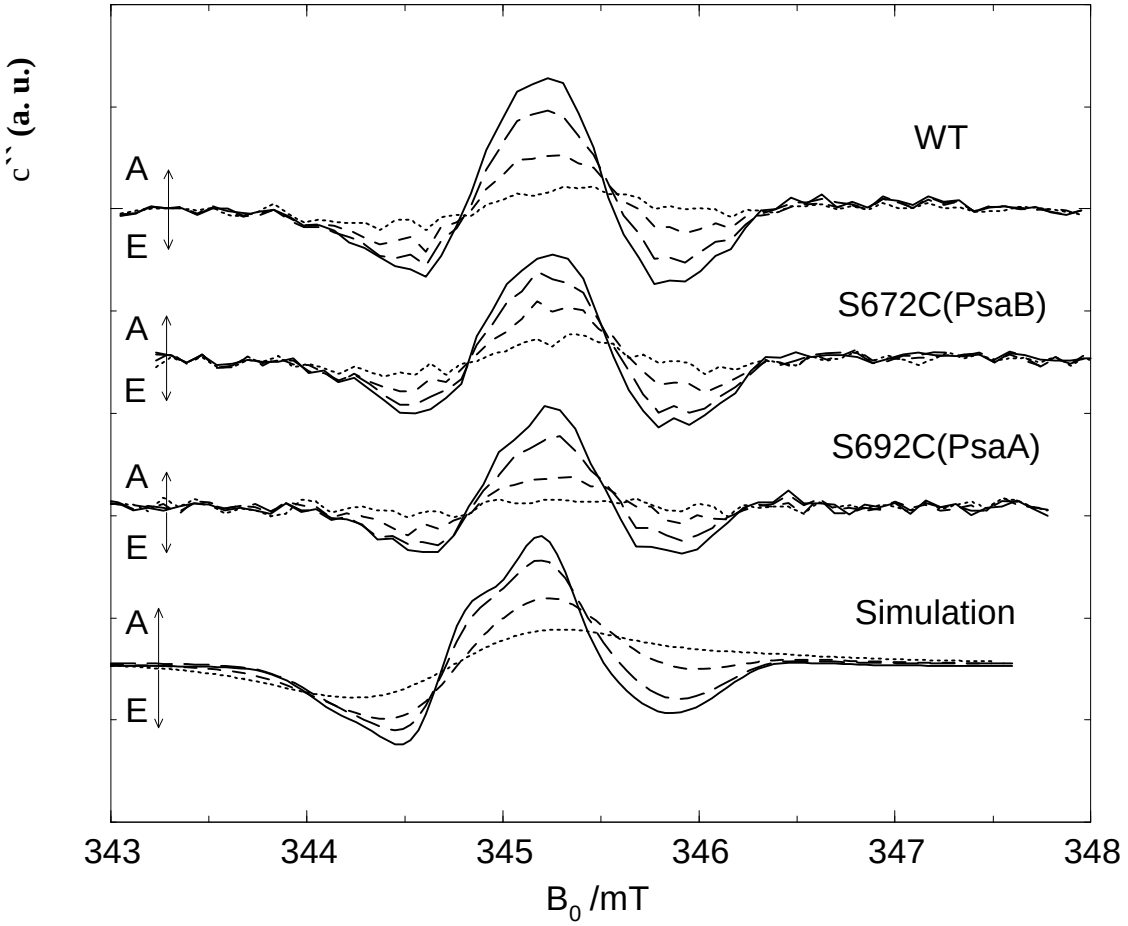

Figure 9.7 Early time development of the spin polarized transient EPR spectra in PS I complexes of the wild-type, $S672C_{PsaB}$ and $S692C_{PsaA}$ mutants at 260 K compared with calculated spectra of the $P_{700}^{+}A_1^{-}$ state (see text for explanation). The spectra are integrated in four successive 16 ns time windows starting 50 ns after the laser flash: 50-66 ns (dotted line), 66-82 ns (short dashed line), 82-98 ns (long dashed line) and 98-114 ns (solid line).

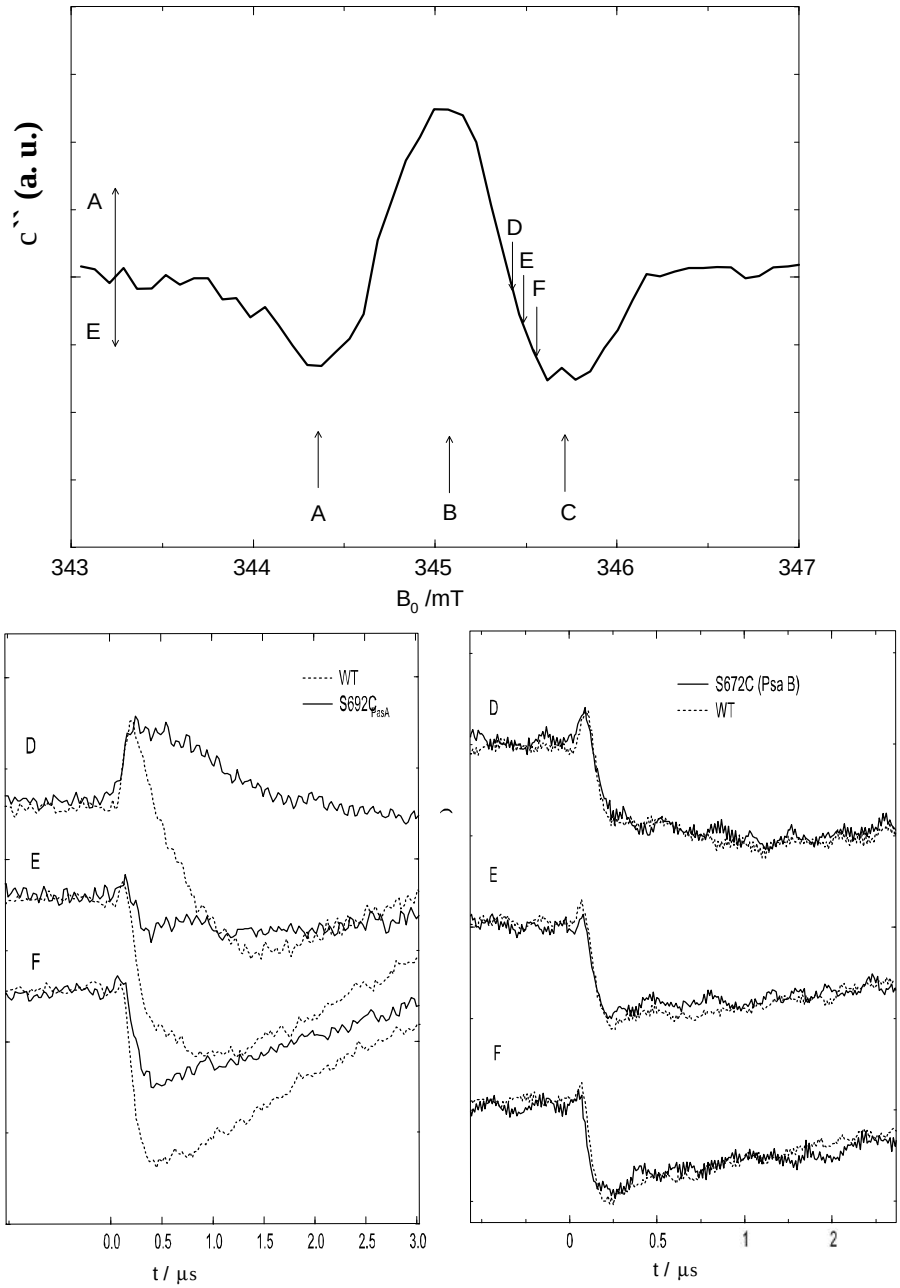

Figure 9.8 Transient EPR kinetic traces at selected magnetic field positions indicated on the spectrum above for S692CPsaA (left) and S672CPsaB (right) compared to wild type PS I at 260K. The arrows D-F in the kinetically separated spectra indicate the field positions selected for transients.

under our experimental conditions and Fourier broadening dominates the early time behavior at the X-band. As is evident in Figure 9.7, the broadening causes an up-field shift of the up-field zero-crossing of the E/A/E polarization pattern. This shift is very well reproduced in numerical simulations (Figure 9.7, bottom) of the $P_{700}^{+}A_1^{-}$ spectrum based on the spin correlated radical pair model [99, 102] in which the signal decay is assumed to be negligibly slow. Thus, it is clear that $P_{700}^{+}A_1^{-}$ dominates the early spectra. Moreover, within experimental error, the net polarization of the experimental spectra at early time is zero. Thus, no evidence is found for spin polarization associated with P_{700}^{+} FeS^{-} from the fast kinetic phase in the electron transfer between A_1^{-} and the iron-sulphur clusters.

This is also confirmed by the selected transients which are shown in Figure 9.6 taken at 260 K for wild-type PS I and the $S672C_{PsaB}$ mutant. The transients at the maxima of the $P_{700}^{+}A_1^{-}$ spectrum (field positions A, B and C indicated on Figure 9.8) are analogous to those measured at room temperature (see Figure 9.3). They do not exhibit any significant difference between the PsaB mutant and the wild type. The transients taken up-field of the zero-crossing point of the $P_{700}^{+}A_1^{-}$ spectrum (positions D, E and F) demonstrate the influence of Fourier broadening by the short (< 100 ns) initial, absorptive (positive) spike in transients D, E and F generated by the shift of the zero-crossing point in the early spectra of Figure 9.8. The positive spike at these field positions can only result from the Fourier-broaden early signal of $P_{700}^{+}A_1^{-}$ state. Any early contribution from P_{700}^{+} FeS^{-} state can only have an emissive (negative) amplitude. Since within experimental accuracy the spike does not change in amplitude between the wild type and both mutants $S672C_{PsaB}$ and $S692C_{PsaA}$ (Figure 9.8), we conclude that the mutations do not cause a measurable change of the early signal for the time range >20 ns.

9.4 Asymmetry of electron transfer in PsaA *versus* PsaB branches

The changes in the $P_{700}^{+}A_1^{-}$ radical pair spectra at room temperature for the Trp and Ser mutants (Figure 9.2) mirror those at low temperature, *i.e.* mutations in PsaB have no effect on the polarisation patterns while those in the PsaA result in visible changes. Therefore we conclude that the EPR spectra measured at room temperature are also dominated by the radical pairs generated by electron transfer along the PsaA branch. Optical experiments reveal a component of electron transfer from A_1 to F_x with a lifetime of ~10 ns and it has been proposed that this corresponds to the electron transfer in the PsaB branch [34, 90], see [35] for a summary. Unfortunately, the assignment of the fast kinetic phase has to be left as an open question, for more extended discussion see [95]. Nevertheless, assuming that both kinetic phases are relevant, we now address the question of what fraction of the electrons follows each kinetic phase. While it is clear that the optical data give a much better estimation of the fraction of fast kinetic phase, there appears to be a problem of consistence with the EPR data. Qualitatively, all of the data are consistent in showing that the slow kinetic phase accounts for the major fraction of all of the electrons. The relative amplitudes of the two phases obtained optically suggest that the slow phase accounts for roughly 70% of the electrons promoted by P_{700}. The EPR data, on the other hand, do not show any clear indication of the fast phase either at room temperature or at 260 K. As discussed above, any net polarization of P_{700}^{+} generated by a fast kinetic phase will last for many microseconds, so there is no issue of time resolution. For the room temperature data on wild type PS I, comparison with simulated EPR spectra lead to the conclusion that at most ~20% of the reaction centers could have a 10 ns electron transfer time [99]. A qualitative demonstration of the effect of the fast component suggested that for larger fractions, the amplitude ratio of the late and the early spectrum

would be larger than observed. This ratio as extracted from the measured data depends on the deconvolution of the data for the instrument response and on the choice of the effective spin relaxation times w_A and w_B of the pairs $P_{700}^{+}A_1^{-}$ and $P_{700}^{+}(FeS)^{-}$, respectively (see Chapter 5.7 and in Ref. [99]). Specifically, w_A is difficult to determine experimentally in intact PS I. The value w_A measured in a sample lacking all three iron-sulphur centers is within error the same as w_B in intact samples measured under the same conditions [27, 99]. Thus, here we have used the same relaxation rate for both radical pairs. However, the presence of the iron-sulphur clusters in the intact sample could conceivably increase the relaxation rate and hence our value of w_A would be underestimated. Because the relative amplitude of the two signals depends on the factor $k + w_A - w_B$ an underestimation of w_A would lead to an underestimation of the amplitude of the late spectrum and hence to an underestimation of a potential fast phase of electron transfer. The independent of the $P_{700}^{+}A_1^{-}$ radical pair decay on the microwave power in wild type PS I [61] indicates that under the conditions used here, k is much larger than w_A. Although it is possible that the two relaxation rates are not the same, it is unlikely that the uncertainty in $w_A - w_B$ is large enough to have any major influence on the relative amplitudes of the two signals in wild type PS I. In the PsaA mutants, however, the values of k are considerably smaller and such effects could become important. The relative amplitudes of the early and late transient EPR spectra do not give an indication of a fast component.

Another quantifiable criterion is the amount of net polarization in the early spectrum. For the pair $P_{700}^{+}A_1^{-}$, the net polarization is virtually zero because of the extremely short lifetime (~30 ps) of the precursor state $P_{700}^{+}A_0^{-}$ [97]. By contrast, $P_{700}^{+}(FeS)^{-}$ shows pronounced emissive polarization of P_{700}^{+} (the contribution from $(FeS)^{-}$ is not visible because it relaxes very rapidly). Hence, the putative formation of $P_{700}^{+}F_X^{-}$ within about 10 ns in a fraction of the reaction centers should be visible as a net emission

of the early EPR spectrum. It was demonstrated that in spinach samples known to contain a large fraction of fast electron transfer the influence of the fast phase is clearly evident [33] in the transient EPR data resulting in a spectrum with net emission at early times. Even though the fast phase signal in this case was preparation induced by treatment of chloroplasts with detergent; there is no doubt that the presence of such a phase can be detected under the proper conditions. Because the strength of the net polarization increases with the lifetime of the precursor state, we had expected that the fast phase in our cyanobacterial samples would become more easily observable, perhaps even directly by EPR, by decreasing the temperature of the sample to 260 K. Yet, as shown in Figures 9.6-9.8 no clear indication of the fast phase was found. However, this is not surprising in the light of a recent optical study on PS I from *Synechocystis* sp. PCC 6803 that showed that the rate of the fast phase was virtually independent of temperature and that its relative amplitude decreased from ~28% at room temperature to ~20% at 260 K [98]. Three other observations at 260 K are relevant, however:

- The early time-behavior of the spin-polarization could be simulated by a spin-correlated radical pair model with the assumption that only $P_{700}^{+}A_1^{-}$ contributed to the early spectra (see Figure 9.7).
- Within experimental error, the net polarization of the spectra at early times was zero (Figure 9.7).
- EPR transients of wild type and $S692C_{PsaB}$ mutant were virtually identical (Figures 9.6, 9.8), although the fast phase as detected optically at room temperature was found to be about two times slower in isolated PS I from this mutant than in wild-type PS I.